Ocean Modelling

Yukiharu Hisaki

Spectral interpolation of long-travelling predicted waves

This is an Author's Accepted Manuscript of an article published in

Ocean Modelling

Volume 38, Issues 3-4, 2011, Pages 217-229

Available online at: https://doi.org/10.1016/j.ocemod.2011.03.003

Spectral interpolation of long-travelling predicted waves

Yukiharu Hisaki[a,*]

[a] *University of the Ryukyus, 1-Aza Senbaru, Nishihara-cho, Okinawa, 903-0213 Japan. Tel. +81-98-895-8515; Fax:+81-98-895-8552*

Abstract

If a swell propagating over a long distance is dominant, existing spectral wave models will produce unphysical oscillations in the model-predicted wave height field as a result of finite spectral resolution. This is called the Garden Sprinkler Effect (GSE), which is more apparent with high-accuracy propagation schemes. Here, an interpolation method to remove the GSE is developed. This method involves retrieving the higher-resolution wave spectra from lower-resolution wave spectra that are predicted not from a GSE-alleviating scheme but from a shape-preserving advection scheme, by considering the spatial distribution of spectra. Using this method both the removal of the GSE and the preservation of the spatial distribution of spectral values can be attained almost completely.

Keywords: Swell; Garden Sprinkler Effect; Numerical modeling; Wave spectrum

*Corresponding author
Email address: hisaki@sci.u-ryukyu.ac.jp (Yukiharu Hisaki)

1. Introduction

It is important to include swell predictions in wave forecasting. A wave spectral energy or action balance equation such as

$$\frac{DF}{Dt} = S \tag{1}$$

can be solved for wave forecasting, where t is a time, F is the ocean wave spectrum, S is the net source function, and D/Dt represents the total derivative moving with the wave component (e.g., Komen et al. (1994)). If we only consider spatial propagation, assuming that other terms may either be neglected or treated separately by time-splitting methods (e.g., WISE Group (2007)), equation (1) reduces to a propagation equation.

The propagation equation in Cartesian (x, y) coordinates for deep water is

$$\frac{\partial F}{\partial t} + \frac{\partial (c_g \cos\theta F)}{\partial x} + \frac{\partial (c_g \sin\theta F)}{\partial y} = 0, \tag{2}$$

where $F = F(\omega, \theta, x, y, t)$ is the ocean wave spectrum at the position (x, y), radian frequency ω, direction θ with respect to the $x-$ direction and time t, and c_g is the group velocity. A shape-preserving advection scheme for solving the propagation equation (2) is required to predict swells that travel a long distance. The term "shape-preserving" means that spatial structure of features in a single spectral component advected in space is maintained by a given numerical scheme.

A high-resolution model is preferred for wave forecasting; however, the limited ability of computers limits the resolution. If the resolutions of wave frequency and direction are coarse, a numerical artifact known as the Garden Sprinkler Effect (GSE) occurs when a swell is propagated over a long distance

(e.g., Booij and Holthuijsen (1987)). The spatial distribution of wave heights cannot be accurately predicted due to this artifact. A GSE-alleviation scheme is necessary to predict the spatial distribution of wave heights. A shape-preserving scheme with insufficient resolution results in the display of the GSE (e.g., WISE Group (2007)), and therefore requires GSE alleviation.

The numerical diffusion is significant for the first-order upwind scheme, and such a scheme is not shape-preserving. The GSE is not clearly seen in the spatial distribution of wave heights for the first-order upwind scheme. Therefore, the first-order upwind scheme is adopted in WAM cycle 4 (Janssen, 2008). However, the numerical diffusion is unrelated to physical dispersion, and this method is not valid as a GSE alleviation method (e.g., WISE Group (2007)).

Some existing schemes to reduce the GSE are based on the spatial averaging of waves at the expense of the shape-preserving property of the high-order-accuracy scheme for the propagation equation. For example, Booij and Holthuijsen (1987) developed a method to alleviate the GSE by adding a diffusion term to equation (2), which is derived to describe sub-grid dispersion in a model with insufficient spectral resolution. Lavrenov and Onvlee (1995) developed a GSE-alleviating method by averaging wave energies of different directions, in which energy may be spread over all directions.

Tolman (2002) developed a GSE-alleviating method by averaging wave energies of different frequencies and directions to improve computational economy. Tolman (2002) also developed a GSE-alleviating method called divergence method. This method consists of adding divergence, representing the difference between spectral bin-mean and spectral bin-centric propaga-

tion, to the advection field.

The spatial distribution of the energy in a single spectral bin becomes smoother for the GSE-alleviating method, while the initial distribution is advected with minimal change of shape for the so-called "plain ULTIMATE QUICKEST scheme," which is almost shape-preserving (Fig. 10 in Tolman (2002)).

We have developed a new method to alleviate the GSE by post-processing spectra from a wave model run which also allows us to retrieve high-resolution spectra. The initial wave shape is almost completely preserved except for the influence of the numerical diffusion of the high-order-accuracy propagation scheme. The method involves interpolating high-resolution wave spectra from low-resolution wave spectra that are predicted not from a GSE-alleviating scheme but from a shape-preserving advection scheme such as the Cubic interpolated propagation (CIP) method (Yabe and Aoki (1991)) or the ULTIMATE QUICKEST scheme (Leonard (1991)).

The GSE is explained in section 2. The method to remove the GSE from predicted wave spectra is presented in section 3. This method is applied to predicted wave spectra both for the ideal case and a practical case in section 4. The advantage of the present method is also demonstrated in section 4. Section 5 presents conclusions and discussions for future explorations of this subject.

2. Garden Sprinkler Effect

Consider equation (2). The solution of equation (2) is

$$F = F_0(\omega, \theta, x - c_g \cos\theta t, y - c_g \sin\theta t), \tag{3}$$

where $F_0 = F_0(\omega, \theta, x, y)$ is the wave spectrum at time $t = 0$.

The variable $(\log(\omega), \theta, x, y, t)$ of the wave spectrum F is discretized in equal steps : The radian frequency is $\omega_{i+1} = r_\omega \omega_i$, where i is the discrete grid index number in ω-space, and r_ω is a constant greater than 1. The wave direction is $\theta_j = -\pi + j\Delta\theta = -\pi + 2\pi j/M$, j is the index number of the direction, $\Delta\theta = 2\pi/M$ is the resolution of the direction, and M is the number of directions. The spatial resolution is $(\Delta x, \Delta y)$, and the time step is Δt.

Wave-height estimation from (3) for two spectral resolutions are shown in Figure 1. The time is $t = 125$ hour, and the initial wave spectrum is

$$F_0(\omega, \theta, x, y) = \frac{H_0^2}{8\pi\sqrt{2\pi}\omega_\sigma} \exp(-\frac{(\omega - \omega_p)^2}{2\omega_\sigma^2})[\max(\cos(\theta - \theta_p), 0)]^2, \qquad (4)$$

where

$$H_0 = H_s \exp(-\frac{r^2}{2r_L^2}) \qquad (5)$$

is the initial wave height, $r^2 = (x - x_0)^2 + (y - y_0)^2$, $(x_0, y_0) = (0, 0)$, $H_s = 2.5$ m, $r_L = 150$ km, $\omega_p/(2\pi) = 0.1$ Hz, $\omega_\sigma/(2\pi) = 0.01$ Hz, and $\theta_p = 30°$. These are almost same parameters as those in Tolman (2002).

The significant wave height is estimated by integrating the wave spectrum F with respect to ω and θ, but the spectral values are estimated only at discretized frequencies ω_i and directions θ_j. The spectral values F at other frequencies and directions are interpolated only in the $\omega - \theta$ plane.

Figure 1a shows the significant wave height from Eqs. (3) and (4) for $r_\omega = 1.1$ and $\Delta\theta = 15°$ ($M = 24$), which is referred to as the coarse-resolution case. The spatial resolution is $\Delta x = \Delta y = 100$ km. The initial wave spectra F_0 at the position of $(x - c_g \cos\theta t,\ y - c_g \sin\theta t)$ (right-hand side of Eq. (3)) are estimated by the bilinear interpolation of $F_0(\omega, \theta, x, y, t)$ in

the $x - y$ plane. The GSE is seen in Figure 1a, even though Eq. (3) is the exact solution of (2).

Figure 1b shows the significant wave height for $r_\omega = 1.1^{1/2}$ and $\Delta\theta = 3^\circ$ ($M = 120$), referred to as the fine-resolution case. The GSE cannot be seen in Figure 1b.

Figure 2 shows the normalized F as a function of wave direction θ at $(\omega/(2\pi), x, y) = (0.1$ Hz, 3000 km, 1800 km) and $(\omega/(2\pi), x, y) = (0.1$ Hz, 3400 km, 1400 km) for the coarse-resolution ($(r_\omega, \Delta\theta) = (1.1, 15^\circ)$) and fine-resolution case ($(r_\omega, \Delta\theta) = (1.1^{1/2}, 3^\circ)$). The values in Figure 2a and b are respectively normalized by the maximum of $F(0.2\pi$ s^{-1}, θ, 3000 km, 1800 km) and $F(0.2\pi$ s^{-1}, θ, 3400 km, 1400 km) for the fine-resolution case.

The sampled spectral values for the coarse-resolution case are equal to those for the fine-resolution case (Figure 2a). If the spectral peak value is sampled in the coarse-resolution case, the integrated value of F with respect to θ is overestimated (Figure 2a). If the spectral peak is not sampled in the coarse-resolution case ($(r_\omega, \Delta\theta) = (1.1, 15^\circ)$), the integrated value of F is underestimated (Figure 2b). Therefore, the GSE occurs as in Figure 1a; the wave heights at positions in the direction of θ_j from $(x, y) = (0, 0)$ are overestimated, and wave heights at other positions are underestimated.

Waves coming from far away are approximately parallel to each other. The directional distribution of the wave spectrum is so narrow that the directional distribution cannot be resolved by the coarse directional resolution. The frequency spectrum for the waves travelling a long distance is also narrow because of the dispersion of the waves.

Equations (3) and (4) give an exact solution of the propagation equation

(2), regardless of any spectral and spatial discretization. Figure 1 shows the significant wave height computed using (3) and (4) only at the discrete frequencies and directions, so the GSE arises from integrating a finite-resolution spectrum with insufficient resolution to resolve the narrow peak, not because of any inexactness in Eq. (3) where it is applied.

Figure 3 shows the contours of the wave spectra $F(\omega, \theta, x, y, t)$ at $(\omega/(2\pi), t)$ = (0.1 Hz, 125 hour). Figure 3a, b and c show the contours of F for the coarse-resolution case at $\theta = 15°$, $\theta = 30°$, and $\theta = 21°$, respectively. Figure 3d, e and f show the contours of F for the fine-resolution case at $\theta = 15°$, $\theta = 30°$, and $\theta = 21°$, respectively. The spectral values at $\theta = 21°$ for the coarse-resolution case (Figure 3c) are estimated by interpolation in the $\omega - \theta$ plane.

The contours of F for $\theta = 15°$ in Figure 3a and in Figure 3d are the same. The contours in Figure 3b are the same as those in Figure 3e. The contour pattern in Figure 3a is similar to that in Figure 3b. The difference between Figures 3a and b is described as largely a horizontal displacement of the whole contour pattern. The contour pattern in Figure 3c is dissimilar to those in Figure 3a and b. On the other hand, the contour pattern in Figure 3f is similar to those in Figure 3d and e except for the position of contours. The contours of F for $\theta = 21°$ are located between those for $\theta = 15°$ and $\theta = 30°$, and the contour levels are also between them. The poor result in Figure 3c is an artifact of the interpolation in spectral space: for all other plots, the exact spectra calculated from (3) and (4) at a single spectral bin are used.

The wave directions in Figure 3a and b neighbor each other in the coarse-resolution case: the difference in the direction is $\Delta\theta = 15°$. In the case of the

GSE, the locations of the wave spectrum contours at neighboring frequencies and directions are different, while they are close to each other in the case without the GSE. In this example, the distance is greater than 3 grid cells when the GSE can be seen.

We can deduce the contour of $\theta = 21^\circ$ from Figure 3d and e as Figure 3f. The method of drawing the contour of F at $\theta = 21^\circ$ from the contours of F at $\theta = 15^\circ$ and $\theta = 30^\circ$ is considered. Figure 3f is valid based on Figure 3d and e.

Our method for removing the GSE is based on a procedure to interpolate the spectral values by spatial distribution of spectra. Both the contour level and the location of the contour pattern are interpolated. This also applies to the interpolation with respect to the wave frequency.

3. Method

3.1. Principle

We consider the interpolation of the spectral values $F(\omega, (\theta_a+\theta_b)/2)$ from $F(\omega, \theta_a)$ and $F(\omega, \theta_b)$ (t or (x, y) is omitted). Figure 4 shows a schematic illustration of the interpolation.

The contour lines of $F(\omega, \theta_a)$ are drawn in the $x-y$ plane as blue curves, and the contour lines of $F(\omega, \theta_b)$ are drawn as red curves in Figure 4. The contour lines of $F(\omega, (\theta_a+\theta_b)/2)$ are located in the middle of those of $F(\omega, \theta_a)$ and $F(\omega, \theta_b)$. The local maximum point of $F(\omega, (\theta_a + \theta_b)/2)$ in the $x - y$ plane (C in Figure 4) is the mid-point of those of $F(\omega, \theta_a)$ (A in Figure 4) and $F(\omega, \theta_b)$ (B in Figure 4), i. e., $\vec{AC} = \vec{CB}$. The spectral value $F(\omega, (\theta_a+\theta_b)/2)$, at the position of C in Figure 4 is interpolated as $F(\omega, (\theta_a + \theta_b)/2, \mathrm{C}) = 1/2$

$[F(\omega, \theta_a, \mathrm{A}) + F(\omega, \theta_b, \mathrm{B})]$. The spectral value at the position R (Figure 4), which is near the position of C, is also interpolated as $F(\omega, (\theta_a + \theta_b)/2, \mathrm{R}) = 1/2\ [F(\omega, \theta_a, \mathrm{P}) + F(\omega, \theta_b, \mathrm{Q})]$, where P and Q are positions satisfying $\vec{AP} = \vec{BQ} = \vec{CR}$ in Figure 4.

Although the points A, B, P and Q in Figure 4 are on grid points in the $x-y$ plane, the interpolated points C and R are not on grid points in the $x-y$ plane. In this case, the spectral values $F(\omega, (\theta_a + \theta_b)/2)$ on the grid points in the $x-y$ plane are interpolated. The interpolation of $F(\omega, (\theta_a + \theta_b)/2)$ by this method is done for the position around C in Figure 4. In other areas of the $x-y$ plane, the spectral values $F(\omega, (\theta_a + \theta_b)/2)$ are interpolated with respect to (ω, θ).

It is possible to interpolate the spectral values $F(\omega_q, \theta_q, x, y)$ from $F(\omega_a, \theta_a, x, y)$, $F(\omega_a, \theta_b, x, y)$, $F(\omega_b, \theta_a, x, y)$, and $F(\omega_b, \theta_b, x, y)$ where ω_q is the radian frequency of $\omega_a < \omega_q < \omega_b$, and θ_q is the direction of $\theta_a < \theta_q < \theta_b$ in the similar way. The details of the interpolation are written in Sections3.2, 3.3 and Appendix A.

3.2. Interpolation of the spectrum

The method to remove the GSE is to estimate the spectrum $F = F_q$ at (ω_q, θ_q), where $\omega_a < \omega_q < \omega_b$, θ_q is in the direction of $\theta_a < \theta_q < \theta_b$, and ($\omega_a$, ω_b, θ_a, θ_b) is

$$\omega_a = \omega_i, \tag{6}$$

$$\omega_b = \omega_{i+1} = r_\omega \omega_i, \tag{7}$$

$$\theta_a = \theta_j, \tag{8}$$

$$\theta_b = \theta_{j+1} = \theta_j + \Delta\theta. \tag{9}$$

Figure 5 shows a schematic illustration of the interpolation of the spectral values. Consider the contour lines of

$$F_{aa} = F(\omega_a, \theta_a, x, y), \qquad F_{ab} = F(\omega_a, \theta_b, x, y), \tag{10}$$

$$F_{ba} = F(\omega_b, \theta_a, x, y), \qquad F_{bb} = F(\omega_b, \theta_b, x, y) \tag{11}$$

in the $x - y$ plane. The P_1, P_2, P_3, and P_4 in Figure 5 are local maxima of F_{aa}, F_{ab}, F_{ba} and F_{bb}, respectively. It may be better to obtain P_2 from P_1 by calculating the cross-correlation between F_{aa} and F_{ab}, but P_2 was obtained by searching for the local maximum of F_{ab} to reduce the computation time.

The $x - y$ coordinate was normalized by Δx, and Δy. The normalized $x-y$ coordinates (grid numbers) of P_1, P_2, P_3, and P_4 are (M_1, N_1), (M_2, N_2), (M_3, N_3), and (M_4, N_4), respectively. The quadrangle $P_1P_2P_3P_4$ is almost a parallelogram, because P_1P_2 is the difference of the wave-travelling distances, and $\Delta\theta$ is much smaller than unity. The groups of the grid points surrounding the contours F_{aa}, F_{ab}, F_{ba}, and F_{bb} are C_1, C_2, C_3, and C_4, respectively (Figure 5).

The areas of C_m $(m = 1, 2, 3, 4)$ were set to be squares with length $2L$ and with centers P_m $(m = 1, 2, 3, 4)$ to code the program easily. The normalized coordinate of C_m $(m = 1, 2, 3, 4)$ is $(q_{m,x}(i), q_{m,y}(j))$, where

$$q_{m,x}(i) = i + M_m, \qquad i = -L, .., 0, .., L \tag{12}$$

$$q_{m,y}(j) = j + N_m, \qquad j = -L, .., 0, .., L \tag{13}$$

which are indicated by green, brown, black and red points in Figure 5.

The group of grid points surrounding the contours F_q is C (blue points in Figure 5). The area of C is a square with the length of $2L$ and with the

center P. The spectral value F_q in the area of C was interpolated from the spectral values F_{aa} in the area of C_1, F_{ab} in the area of C_2, F_{ba} in the area of C_3, and F_{bb} in the area of C_4.

3.3. Summary of the method

The procedure for estimating the spectrum $F = F_q$ at (ω_q, θ_q) can be summarized as follows:

1. The local maximum positions of $F_{aa} = F(\omega_a, \theta_a, x, y)$, $F_{ab} = F(\omega_a, \theta_b, x, y)$, $F_{ba} = F(\omega_b, \theta_a, x, y)$, and $F_{bb} = F(\omega_b, \theta_b, x, y)$ in the $x - y$ plane P_m $(m = 1, 2, 3, 4)$ are obtained, identified on Figure 5 as points P_m $(m = 1, 2, 3, 4)$,
2. If there are multiple local maxima of the spectral value in the $x - y$ plane, the groups of P_m are selected so as to minimize the distance between them.
3. If the positions P_m are close to each other to within order 3 grid cells, the spectrum $F = F_q$ at (ω_q, θ_q) is interpolated only in the $\omega - \theta$ plane.
4. Otherwise, the spectrum $F = F_q$ at (ω_q, θ_q) is interpolated as explained below, and in more detail in Appendix A.1 and Appendix A.2.
5. An equal-sized square spatial subgrid is defined around each of the four local maxima P_m, containing grid cells $(q_{m,x}(i)q_{m,y}(j))$, for $(i, j = -L, .., 0, .., L)$ (Eqs. (12) and (13)). The length L is set to the maximum value that ensures that at least one of the four subgrids contains only spectral densities F greater than ϵ times the local peak value, where ϵ is a tunable parameter. A more detailed definition of L is given in Equations (A.28) and (A.29) of the Appendix A.2. An adjustable global upper limit L_{th} is also set on the value of L.

6. A pair of subgrid indices (i, j) corresponds to the points Q_m $(m = 1, ..., 4)$ on the four subgrids (Figure 5). We define a corresponding point Q for the target spectral coordinates (ω_q, θ_q), located at the interpolated spatial grid coordinates:

$$(q_x(i), q_y(j)) = \sum_{m=1}^{4} W_m(q_{m,x}(i), q_{m,y}(j)) \tag{14}$$

with weights W_m given by bilinear interpolation in ω and θ as detailed by Equations (A.3)–(A.6) in Appendix A.1.

7. The spectral density F at Q is interpolated using the same weights, i.e.,

$$F(\omega_q, \theta_q, q_x(i), q_y(j)) = \sum_{m=1}^{4} W_m F(\omega_{abm}, \theta_{abm}, q_{m,x}(i), q_{m,y}(j)) \tag{15}$$

where

$$\omega_{ab1} = \omega_{ab2} = \omega_a, \qquad \omega_{ab3} = \omega_{ab4} = \omega_b, \tag{16}$$

$$\theta_{ab1} = \theta_{ab3} = \theta_a, \qquad \theta_{ab2} = \theta_{ab4} = \theta_b. \tag{17}$$

8. The grid coordinates $(q_x(i), q_y(j))$ do not in general correspond to the integer values required for final output. Hence a final step of bilinear spatial interpolation of the spectrum is required from the grid consisting of the set of points $\{(q_x(i), q_y(j)), i, j = -L, ..., 0, ..., L\}$ to the parts of the integer-valued output grid lying within it. Outside this region, the spectral values F_q are obtained by interpolation in the $\omega - \theta$ plane. More details of this interpolation are given in Appendix A.2.

The interpolation is done from spatially correlated areas of wave spectra. The contour patterns of wave spectra $F(\omega_{abm}, \theta_{abm})$ in C_m $(m = 1, 2, 3, 4)$,

are similar to each other, which means that the wave spectra in the area are spatially correlated, where $(\omega_{abm}, \theta_{abm})$ are given in Eqs. (16) and (17), and C_m are shown in Figure 5 . The areas C_m $(m = 1, 2, 3, 4$) should be determined to maximize the cross correlations of F_{aa}, F_{ab}, F_{ba}, and F_{bb} (Eqs. (10) and (11)) and the relation (A.29); however, the calculation of the cross-correlation is omitted to reduce the computation time. The method described in this section is called the space correlation interpolation method (SCIM).

4. Results

4.1. Ideal case

Figure 6 shows examples of the application of the SCIM. The wave parameters are the same as those in Figure 1a. The spectra F were estimated from Eq. (3) for the coarse-resolution case $((r_\omega, \Delta\theta) = (1.1, 15^\circ))$, and the SCIM was applied to remove the GSE.

The frequency resolution and direction resolution of interpolated spectra were $r_\omega = 1.1^{1/2}$, and $\Delta\theta = 0.5^\circ$. It was impossible to store the array $F(\omega, \theta, x, y)$ in the memory of our personal computer for such a high-resolution spectrum. However, it was unnecessary to save the array $F(\omega, \theta, x, y)$ in the computer memory only for estimating wave parameters.

The parameter ϵ in (A.29) is $\epsilon = 10^{-2}$ in Figure 6a. The maximum value of L, which varies with $(\omega_a, \theta_a) = (\omega_i, \theta_j)$, is 5. The GSE is removed in Figure 6a, but the removal is incomplete. The local maxima of the wave heights can be seen in Figure 6a.

The parameter ϵ in Eq. (A.29) is $\epsilon = 10^{-10}$ in Figure 6b. The maximum

value of L is 9. The GSE is almost completely removed in Figure 6b except near the boundary in Figure 6b. The SCIM is done within the area of $-1000 \leq x, y \leq 4500$ km, and the spectra near the boundary are not interpolated.

There are no effects of local winds on waves in the ideal case. Therefore, the parameter ϵ (Eq. (A.29)) must be small, and L must be large, because spectra on the area outside the C (Figure 5) are interpolated only on the $\omega - \theta$ plane. If the spectral values outside C are set to be 0, the GSE can be almost completely removed for larger ϵ. However, the real waves are affected by local winds, and it is necessary to set the parameter ϵ larger than 10^{-10}.

4.2. Advantage of the SCIM

Figure 7 shows the comparison of wave spectra $F(\omega, \theta)$ at $(x, y) = (3000\,\text{km}, 1800\,\text{km})$. Figure 7a is the wave spectrum obtained from the low-resolution spectra ($(r_\omega, \Delta\theta) = (1.1, 15^\circ)$) by the SCIM. Figure 7b is the wave spectrum obtained from (3) and (4). The initial wave spectra F_0 at the position of $(x - c_g \cos\theta t,\ y - c_g \sin\theta t)$ (right-hand side of Eq. (3)) were estimated from (4) and not from the bilinear interpolation in the $x - y$ plane. The spectral resolution was $(r_\omega, \Delta\theta) = (1.1^{1/2}, 0.5^\circ)$. Figure 7c is the wave spectrum obtained from (3). The initial wave spectra at the position of $(x - c_g \cos\theta t,\ y - c_g \sin\theta t)$ were estimated from the bilinear interpolation, and the spectral resolution was $(r_\omega, \Delta\theta) = (1.1^{1/2}, 1^\circ)$. Figure 7d is the wave spectrum for the coarse-resolution case ($(r_\omega, \Delta\theta) = (1.1, 15^\circ)$).

The wave spectral distribution is broad and the wave energy is overestimated for the coarse-resolution case (Figure 7d). The wave spectrum retrieved by the SCIM (Figure 7a) is similar to both Figure 7b and c. However, the spectral peak values of Figure 7a and c are smaller than that of

Figure 7b, because the spatial resolution ($\Delta x = \Delta y = 100$ km) is not enough to resolve the initial wave height distribution, whose width r_L (Eq. (5)) is 150 km. Although there are some differences, it is shown that the SCIM can retrieve high-resolution spectra from low-resolution spectra.

Figure 8 shows wave spectra $F(\omega, \theta)$ at $(\omega/(2\pi), \theta) = (0.1(1.1)^{1/2}\text{Hz}, 25^\circ)$ for t = 8.3, 50, 91.6 and 133.3 hours retrieved by the SCIM. The spectral values at $(\omega/(2\pi), \theta) = (0.1(1.1)^{1/2}\text{Hz}, 25^\circ)$ were interpolated from $F(\omega_i, \theta_j)$, $F(\omega_i, \theta_{j+1})$, $F(\omega_{i+1}, \theta_j)$, $F(\omega_{i+1}, \theta_{j+1})$ for the coarse-resolution case ($(r_\omega, \Delta\theta) = (1.1, 15^\circ)$), where $\omega_i/(2\pi) = 0.1$ Hz, and $\theta_j = 15^\circ$. The contour patterns are advected along the 25° line (dashed line in Figure 8). If the shape-preserving advection scheme is used, there is no spectral dispersion in the present method. The advantages of the SCIM are that a spectral value at a single spectral bin is preserved (Figure 8), and that it is possible to estimate high-resolution spectra (Figure 7).

4.3. Case of dual swell systems

The case of dual swell systems passing across each other is investigated. The initial wave spectra for one of the swell systems were the same as those in Figure 1 (Eqs. (4) and (5)) and parameters of them). The other initial wave spectra were also described by Eqs. (4) and (5) but for $(x_0, y_0) = (0, 3000\text{ km})$, $H_s = 2.1$ m, $r_L = 135$ km, and $\omega_p/(2\pi) = 0.11$ Hz. The swell directions at the position (x, y) $(x > 0)$, which is far from the swell sources, are $\text{Arctan}(y/x)$ and $\text{Arctan}((y - y_0)/x)$ ($y_0 = 3000$ km).

Figure 9a is the predicted wave height for the coarse-resolution case (t = 125 hour). The directional GSE from $(x, y) = (0, 0)$ and $(x, y) = (0, 3000\text{ km})$ can be seen in Figure 9a. Figure 9b is the predicted wave height for the fine-

resolution case, and the GSE cannot be seen in Figure 9b. Figure 9c is the wave height estimated by the SCIM. There are cases in which the $F(\omega_i, \theta_j)$ in the $x-y$ plane has two local maxima associated with different swell systems. In these cases, the group of local maxima (P_1, P_2, P_3, and P_4 in Figure 5) were selected so as to be as close to each other as possible (step 2 in section 3.3). The GSE was removed in Figure 9c.

4.4. Practical application

The wave model was run and wave spectra were predicted. The source function of the energy balance equation was the same as that of the WAM cycle 4 (e.g., WISE Group (2007); Janssen (2008)), and the propagation term was transferred to a spherical grid (e.g., WAMDI Group (1988)). The cubic interpolated propagation (CIP) method (Yabe and Aoki (1991)), which preserves the waveform almost completely, was used to solve the propagation equation. The spatial resolution was 0.5°, and the spectral resolution was $(r_\omega, \Delta\theta) = (1.1, 15°)$. The ECMWF ERA-Interim surface wind data were used to predict wave data.

In practical conditions, swells are not generally the major source of local wave energy. Therefore, the GSE is unclear in the contour map of the significant wave height (e.g., Tolman (2002)). The peak period is the indicator of the GSE.

Figure 10 shows the predicted peak period $T_p = 2\pi/\omega_p$ and peak direction θ_p, where (ω_p, θ_p) maximizes the $F(\omega, \theta)$, in the northwest Pacific Ocean at 6 UT on May 22, 2008. The GSE can be seen in Figure 10. The peak wave directions in the area where ocean swells reach are scattered. For example, the peak wave direction is southeastward at (17° N, 140° E), where the peak

period T_p is about 10 s. The peak wave direction is southwestward at (12° N, 140° E).

A storm passed near the Pacific coast of Japan, and a swell was generated by the storm. The position of the storm was (30° N , 133° E) on May 20, 2008, with a wind speed greater than 20 m/s.

Figure 11 shows the wave spectra $F(\omega, \theta)$ at $(\omega/(2\pi), \theta) = (0.0751$ Hz, $-60°)$, (0.0751 Hz, $-45°$), (0.0826 Hz, $-60°$), and (0.0826 Hz, $-45°$). The frequencies and directions are adjacent to each other for the coarse-resolution case ($(r_\omega, \Delta\theta) = (1.1, 15°)$). The positions of the contours are significantly different from each other, in particular, for neighboring directions. The SCIM must be applied to estimate wave spectra $F(\omega, \theta)$ for $0.0751 < \omega/(2\pi) <$ 0.0826 Hz and $-60° < \theta < -45°$.

Figure 12 shows the peak period T_p and peak direction θ_p at 6 UT on May 22, 2008. The SCIM was applied to the predicted wave spectra. The value of ϵ in (A.29) was 0.1, which is larger than that for the ideal case, because wave spectra are affected by local winds. The width $2L$ of C_m ($m = 1, 2, 3, 4$, Figure 5) was not determined only from (A.29), and the parameter L_{th} was 25.

The resolution of the wave spectrum was $(r_\omega, \Delta\theta) = (1.1^{1/2}, 0.5°)$. The peak frequencies ω_p and directions θ_p were searched for from the high-resolution spectra. The GSE could be removed in Figure 12. The propagation of the swell from the center of the storm was predicted. The contour lines of $T_p > 11$ s are almost concentric circles, and peak wave directions are in the radial direction of the circles.

5. Discussion and conclusions

If the wave frequency or direction resolution is too coarse to resolve a narrow-band wave spectrum, the GSE appears. In this work, a new method is developed to remove the GSE. In previous studies (e.g., Booij and Holthuijsen (1987); Tolman (2002)), the spectrum at the radian frequency ω and the direction θ is considered to be the average of the spectral values in the frequency and direction band. In these studies the GSE is alleviated by either introducing diffusion terms (Booij and Holthuijsen (1987)), or by spatial averaging of each spectral component (Tolman (2002)).

On the other hand, the SCIM is intended to retrieve a high-spectral-resolution spectrum from a low-spectral-resolution spectrum. The problem of the GSE being more apparent with propagation schemes of higher-order accuracy is resolved by the SCIM. The wave spectra were calculated without a GSE-alleviating method. No additional computing time was required for computing the wave spectra. The SCIM can be applied to archived wave spectra when GSE occurs. Because data storage is limited, it is better to apply the SCIM only where necessary. However, the additional computation time of the post-processing is required.

The positions of the contour patterns of spectral values of neighboring frequencies and directions are indicators of the GSE. If the positions differ from each other, GSE occurs. The spectral values at sampled frequencies and directions were not modified. There was no spatial smoothing of the spectra. Although there are no physics in the SCIM, the SCIM is more valid for interpolating wave spectra than interpolation on the $\omega - \theta$ plane.

There are some issues to be addressed. The first is how we decided the

length L (Eqs. (12),(13)), where $2L$ is the width of C_m ($m = 1, 2, 3, 4$, Figure 5), because the SCIM is dependent on L.

The second is that the SCIM was applied near a coastal area. The areas of C_m ($m = 1, 2, 3, 4$) are assumed to be square with the center of local maxima P_m ($m = 1, 2, 3, 4$). It is assumed that the contour patterns of F_{aa}, F_{ab}, F_{ba}, and F_{bb} (Eqs. (10) and (11)) are similar to each other. However, if C_m ($m = 1, 2, 3, 4$) is the square, the land may be included in C_m. If the land is a small isolated island, it is possible to interpolate a spectral value on the grid point. However, if the land is not a small isolated island, the assumption that contour patterns of F_{aa}, F_{ab}, F_{ba}, and F_{bb} are similar to each other is not valid. In this case, the areas C_m are not squares to avoid the land. The areas C_m were determined to maximize the cross correlations of F_{aa} in C_1, F_{ab} in C_2, F_{ba} in C_3, and F_{bb} in C_4. In addition, these spectral values on the boundaries of C_m must be much smaller than the local maxima of the spectra.

The third is the effect of the GSE on the source function. The wave model was run without a GSE-correcting scheme, so some source function may have been affected by the GSE. It is not economical computationally to apply the SCIM in every time step. However, issues have also been raised for GSE-correcting schemes in previous studies, because the shapes of the spectra are modified and broadened from the narrow band spectrum. Without a GSE-correcting scheme, the narrow band spectral values are sampled at a coarse frequency and direction step; with a GSE-correcting scheme in the previous studies, the narrow band spectral values are averaged within broad frequency and direction bands. The use of a previous GSE alleviation method with the

SCIM may resolve the problems. These problems are the subjects of future studies.

Acknowledgments

This study was financially supported by a Grant-in-Aid for Scientific Research (C-2) from the Ministry of Education, Culture, Sports, Science, and Technology of Japan (20540429). ECMWF ERA-Interim data used in this study were obtained from the ECMWF data server. The GFD DENNOU Library (available online at http://www.gfd-dennou.org/arch/dcl/) was used for drawing the figures. Comments from the anonymous reviewers were helpful in improving the manuscript.

References

Booij, N., Holthuijsen, L.H., 1987. Propagation of ocean waves in discrete spectral wave models. Journal of Computational Physics, 68, 307-326.

Janssen P. A. E. M., 2008. Progress in ocean wave forecasting Journal of Computational Physics, 227, 3572-3594.

Komen, G. I., L. Cavaleri, M. Donelan, K. Hasselmann, S. Hasselmann and P. A. E. M. Janssen, 1994. Dynamics and Modelling of Ocean Waves. Cambridge Univ. Press, 532 pp.

Lavrenov I. V. and J. R. A. Onvlee 1995. A comparison between the results of wave energy propagation of the WAM model and the interpolation-ray method. Russian Meteorology and Hydrology 3, 29-42.

Leonard, B. P. 1991. The ULTIMATE conservative difference scheme applied to unsteady one-dimensional advection. Computational Methods in Applied Mechanical Engineering 88, 17-74.

The WISE Group, 2007. Wave modelling−The state of the art. Progress in Oceanography, 75, 603-674.

Tolman, H. L., 2002. Alleviating the garden sprinkler effect in wind wave models. Ocean Mod. 4, 269-289.

WAMDI Group, 1988. The WAM model. A third generation ocean wave prediction model. Journal of Physical Oceanography 18, 1775-1809.

Yabe T and T. Aoki, 1991. A universal solver for hyperbolic-equations by cubic-polynomial interpolation. I. One-dimensional solver. Computer Physics Communications, 66, 219-232.

Appendix A. Detailed description of the method

Appendix A.1. Weights for the interpolation

The spectral values at (ω_a, θ_a), (ω_a, θ_b), (ω_b, θ_a), and (ω_b, θ_b), for the coarse-resolution case were almost accurate, where (ω_a, ω_b, θ_a, θ_b) is shown in Eqs. (6)–(9). The spectral values $F_q = F(\omega_q, \theta_q, x, y)$, where ω_q is the radian frequency of $\omega_a < \omega_q < \omega_b$, and θ_q is the direction of $\theta_a < \theta_q < \theta_b$, were interpolated from the spectral values for the coarse-resolution case.

The local maximum grid point of contour F_q is P (Figure 5), and the position in the normalized coordinate is (q_{cx}, q_{cy}), where

$$q_{cx} = \sum_{m=1}^{4} W_m M_m, \tag{A.1}$$

$$q_{cy} = \sum_{m=1}^{4} W_m N_m. \tag{A.2}$$

The weight W_m $(m = 1, 2, 3, 4)$ is

$$W_1 = \frac{(\theta_b - \theta_q)}{\Delta\theta} \frac{\log(\omega_b/\omega_q)}{\log(r_\omega)}, \tag{A.3}$$

$$W_2 = \frac{(\theta_q - \theta_a)}{\Delta\theta} \frac{\log(\omega_b/\omega_q)}{\log(r_\omega)}, \tag{A.4}$$

$$W_3 = \frac{(\theta_b - \theta_q)}{\Delta\theta} \frac{\log(\omega_q/\omega_a)}{\log(r_\omega)}, \tag{A.5}$$

$$W_4 = \frac{(\theta_q - \theta_a)}{\Delta\theta} \frac{\log(\omega_q/\omega_a)}{\log(r_\omega)}. \tag{A.6}$$

The spectral value F_q at the point Q with the position of $(q_x(i), q_y(j))$, $(i, j = -L, ..0, .., L)$ in the normalized $x - y$ coordinate in Figure 5 was interpolated from the spectral values F_{aa} at the point Q_1, F_{ab} at the point Q_2, F_{ba} at the point Q_3, and F_{ab} at the point Q_4 from Eqs. (15), (16) and (17).

Appendix A.2. Interpolation on wave grids in the $x - y$ plane

The points $(q_x(i), q_y(j))$ may not be on the grid points as in Figure 5 (step 8 in section 3.3). The interpolation of the wave spectrum estimated from Eq. (15) on the wave grid point is necessary. Figure 13 shows the schematic interpolation of F_q at $(q_x(i), q_y(j))$ on wave grid points (red points).

In the case that

$$q_{cx} = I_{cx}, \qquad \text{and} \quad q_{cy} = I_{cy}, \tag{A.7}$$

where

$$I_{cx} = \text{int}(q_{cx}), \qquad \text{and} \quad I_{cy} = \text{int}(q_{cy}), \tag{A.8}$$

the spectral values F_q on the grid points $(q_x(i), q_y(j))$ as

$$q_x(i) = i + I_{cx}, \qquad i = -L, .., 0, .., L \tag{A.9}$$

$$q_y(j) = j + I_{cy}, \qquad j = -L, .., 0, .., L \tag{A.10}$$

are estimated by Eq. (15).

In the case that

$$q_{cx} = I_{cx}, \qquad \text{and} \quad q_{cy} \neq I_{cy} \tag{A.11}$$

(Figure 13b and e), the interpolation of F_q at $(q_x(i), q_y(j))$ on wave grid points is derived from the length of AR and AQ in Figure 13e as

$$\begin{aligned} F(\omega_q, \theta_q, i + I_{cx}, j + 1 + I_{cy}) = {} & w_1 F(\omega_q, \theta_q, q_x(i), q_y(j)) \\ & + w_2 F(\omega_q, \theta_q, q_x(i), q_y(j+1)) \end{aligned} \tag{A.12}$$

$$i = -L, .., 0, .., L,$$

$$j = -L, .., 0, ., L-1 \tag{A.13}$$

where

$$w_1 = q_{cy} - I_{cy} \tag{A.14}$$

$$w_2 = 1 - q_{cy} + I_{cy}. \tag{A.15}$$

The right-hand side of Eq. (A.12) is estimated from Eq. (15).

In the case that

$$q_{cx} \neq I_{cx}, \qquad \text{and} \quad q_{cy} = I_{cy} \tag{A.16}$$

(Figure 13c), F_q on the wave grid is estimated as

$$\begin{aligned} F(\omega_q, \theta_q, i + 1 + I_{cx}, j + I_{cy}) = {} & w_1 F(\omega_q, \theta_q, q_x(i), q_y(j)) \\ & + w_2 F(\omega_q, \theta_q, q_x(i+1), q_y(j)), \end{aligned} \tag{A.17}$$

$$i = -L, .., 0, .., L-1,$$
$$j = -L, .., 0, .., L \tag{A.18}$$

where

$$w_1 = q_{cx} - I_{cx} \tag{A.19}$$
$$w_2 = 1 - q_{cx} + I_{cx}. \tag{A.20}$$

The right-hand side of Eq. (A.17) was estimated from Eq. (15).

In the case that

$$q_{cx} \neq I_{cx}, \qquad \text{and} \quad q_{cy} \neq I_{cy} \tag{A.21}$$

(Figure 13d and f), F_q on the wave grid was estimated as

$$\begin{aligned} F(\omega_q, \theta_q, i+1+I_{cx}, j+1+I_{cy}) = {} & w_{11} F(\omega_q, \theta_q, q_x(i), q_y(j)) \\ & + w_{21} F(\omega_q, \theta_q, q_x(i+1), q_y(j)) \\ & + w_{12} F(\omega_q, \theta_q, q_x(i), q_y(j+1)) \\ & + w_{22} F(\omega_q, \theta_q, q_x(i+1), q_y(j+1)) \end{aligned} \tag{A.22}$$

$$i = -L, ..0, .., L-1,$$
$$j = -L, .., 0, .., L-1, \tag{A.23}$$

where

$$w_{11} = (q_{cx} - I_{cx})(q_{cy} - I_{cy}), \tag{A.24}$$
$$w_{21} = (1 - q_{cx} + I_{cx})(q_{cy} - I_{cy}), \tag{A.25}$$
$$w_{12} = (q_{cx} - I_{cx})(1 - q_{cy} + I_{cy}), \tag{A.26}$$
$$w_{22} = (1 - q_{cx} + I_{cx})(1 - q_{cy} + I_{cy}). \tag{A.27}$$

The right-hand side of Eq. (A.22) was estimated from Eq. (15).

Wave spectra at (ω_q, θ_q) estimated from Eq. (15) or Eq. (A.12) or Eq. (A.17) or Eq. (A.22) are only on positions surrounded by C in Figure 5 or red points in Figure 13a–d. Wave spectra F_q at other points are interpolated on the $\omega - \theta$ plane.

The length of C_m ($m = 1, 2, 3, 4$, Figure 5) is a tunable parameter, which was determined from

$$L = \max(L_1, L_2, L_3, L_4). \tag{A.28}$$

The parameter L_m was the maximum value satisfying

$$F(\omega_{abm}, \theta_{abm}, q_{m,x}(i), q_{m,y}(j)) > \epsilon \max(F(\omega_{abm}, \theta_{abm}, q_{m,x}(i), q_{m,y}(j))) \tag{A.29}$$

for all $i = -L_m, ..0, .., L_m$ and $j = -L_m, .., 0, .., L_m$ ($m = 1, 2, 3, 4$), where ϵ is a tunable parameter. The right-hand side of (A.29) $\max(F(\omega_{abm}, \theta_{abm}, q_{m,x}(i), q_{m,y}(j)))$ represents the local maxima of $F(\omega_a, \theta_a, x, y)$ ($m = 1$), $F(\omega_a, \theta_b, x, y)$ ($m = 2$), $F(\omega_b, \theta_a, x, y)$ ($m = 3$), and $F(\omega_b, \theta_b, x, y)$ ($m = 4$). The value of L_m may not be determined only by (A.29). In this case, $L_m = L_{th}$, where L_{th} is the maximum threshold of L_m, and a tunable parameter.

Figure captions

Figure 1: Wave height predicted from Eq. (3) for the (a) coarse-resolution ($(r_\omega, \Delta\theta) = (1.1, 15^\circ)$), and (b) fine-resolution cases ($(r_\omega, \Delta\theta) = (1.1^{1/2}, 3^\circ)$). The contours near $(x, y) = (0, 0)$ are those of the initial wave heights H_0 (Eq. (5)). Unit=m.

Figure 2: Normalized F at (a) $(\omega/(2\pi), x, y)$ = (0.1 Hz, 3000 km, 1800 km), and (b) $(\omega/(2\pi), x, y)$ = (0.1 Hz, 3400 km, 1400 km) for the fine-resolution (blue) and coarse-resolution cases (red).

Figure 3: Wave spectra F (Eq. (3)) at $(\omega/(2\pi), t)$ = (0.1 Hz,125 hour) and at (a) $\theta = 15^\circ$, (b) $\theta = 30^\circ$, and (c) $\theta = 21^\circ$ for the coarse-resolution case. (d) Same as (a) but for the fine-resolution case, (e) same as (b) but for the fine-resolution case, and (f) Same as (c) but for the fine-resolution case. Unit= $\mathrm{m}^2 \cdot s \cdot \mathrm{rad}^{-1}$.

Figure 4: Schematic illustration of the interpolation $F(\omega, (\theta_a + \theta_b)/2)$ from $F(\omega, \theta_a)$ and $F(\omega, \theta_b)$ in the $x-y$ plane. The blue and red contour lines are contour plots of $F(\omega, \theta_a)$ and $F(\omega, \theta_b)$, respectively. The green dashed contour lines are contour plots of $F(\omega, (\theta_a+\theta_b)/2)$, as interpolated from $F(\omega, \theta_a)$ and $F(\omega, \theta_b)$. The points A, B, C are local maxima of $F(\omega, \theta_a)$, $F(\omega, \theta_b)$, and $F(\omega, (\theta_a + \theta_b)/2)$, respectively.

Figure 5: Schematic illustration of the interpolation. The grid line (dashed line) was the grid for wave modeling in the $x - y$ plane, and wave spectra on the grids were estimated. The green, brown, black and red contour lines are contour plots of F_{aa}, F_{ab}, F_{ba}, and F_{bb}, respectively. The P_1, P_2, P_3, and P_4 are local maximum positions of F_{aa}, F_{ab}, F_{ba} and F_{bb}, respectively. The groups of wave grid points C_1, C_2, C_3, and C_4 are wave grid points surrounding the contours of F_{aa}, F_{ab}, F_{ba} and F_{bb}, respectively. The value of F_q at Q, the position of which was interpolated from the positions of Q_m $(m = 1, 2, 3, 4)$, was interpolated from the values of F_{aa} at Q_1, F_{ab} at Q_2, F_{ba} at Q_3 and F_{bb} at Q_4, respectively. The points in C (blue points) were interpolated from the grid positions in C_m $(m = 1, 2, 3, 4)$. The values of F_q on the points in C (blue points) were interpolated from the values of F_{aa} on the grids in C_1, F_{ab} on the grids in C_2, F_{ba} on the grids in C_3, and F_{bb} on the grids in C_4, respectively.

Figure 6: The wave height was predicted from Eq. (3) and SCIM was applied to the wave spectra for (a) $\epsilon = 10^{-2}$ and (b) $\epsilon = 10^{-10}$

Figure 7: Wave spectra $F(\omega, \theta)$ as a function of $\omega/(2\pi)$ and θ at $(x, y, t) =$ (3000 km, 1800 km, 125 hour) obtained from (a) the SCIM, (b) equations (3) and (4), (c) equations (3) and bilinear interpolation in the $x - y$ plane $((r_\omega, \Delta\theta) = (1.1^{1/2}, 0.5^\circ))$, (d) the same as (c) but for the coarse-resolution case. Unit= $\mathrm{m}^2 \cdot s \cdot \mathrm{rad}^{-1}$.

Figure 8: Wave spectra $F(\omega, \theta)$ at $(\omega/(2\pi), \theta) = (0.1(1.1)^{1/2}\mathrm{Hz}, 25^\circ)$ for $t =$ 8.3, 50, 91.6 and 133.3 hour (from left to right contour plots). Unit= $\mathrm{m}^2 \cdot s \cdot \mathrm{rad}^{-1}$. dashed line: 25° lines with respect to the x-direction.

Figure 9: (a) Same as Figure 1a ($(r_\omega, \Delta\theta) = (1.1, 15^\circ)$) but for the dual swell systems case. The contours like circles near $(x, y) = (0, 0)$ and $(x, y) = (0, 3000$ km), are those of the initial wave heights H_0. (b) Same as Figure 1b ($(r_\omega, \Delta\theta) = (1.1^{1/2}, 3^\circ)$) but for the dual swell systems case. (c) Wave heights obtained from the SCIM. Unit= m.

Figure 10: Predicted peak wave periods (Unit=s) and peak wave directions (arrows) in the northwest Pacific Ocean at 6 UT on May 22, 2008.

Figure 11: Predicted wave spectra in the area of $130^\circ - 150^\circ$ E and $10^\circ - 30^\circ$ at 6 UT on May 22, 2008 at (a) $(\omega/(2\pi), \theta) = (0.0751$ Hz, $-60^\circ)$, (b) $(\omega/(2\pi), \theta) = (0.0751$ Hz, $-45^\circ)$, (c) $(\omega/(2\pi), \theta) = (0.0826$ Hz, $-60^\circ)$, and (d) $(\omega/(2\pi), \theta) = (0.0826$ Hz, $-45^\circ)$. Unit= $\mathrm{m}^2 \cdot s \cdot \mathrm{rad}^{-1}$.

Figure 12: Same as Figure 10 but the SCIM is applied.

Figure 13: Schematic illustration of the interpolation. The grid line (solid line) is a grid for wave modeling in the $x - y$ plane, and wave spectra on the grids are estimated. The blue points correspond to blue points in Figure 5, and $(q_x(i), q_y(j))$ in Eq. (14). The red points are grid points for which the spectral values were interpolated from those on blue points. (a) In the case of (A.8), the red points are $(i + I_{cx}, j + I_{cy})$ $(i, j = -L, .., 0, .., L)$, (b) in the case of (A.11), the red points are $(i + I_{cx}, j + 1 + I_{cy})$ $(i = -L, .., 0, .., L$, $j = -L, .., 0, .., L - 1)$, (c) in the case of (A.16), the red points are $(i + 1 + I_{cx}, j + I_{cy})$ $(i = -L, .., 0, .., L - 1$, $j = -L, .., 0, .., L)$, and (d) in the case of (A.21), the red points are $(i + 1 + I_{cx}, j + 1 + I_{cy})$ $(i = -L, .., 0, .., L - 1$, $j = -L, .., 0, .., L - 1)$. (e) Extended view of (b), and (f) extended view of (d).

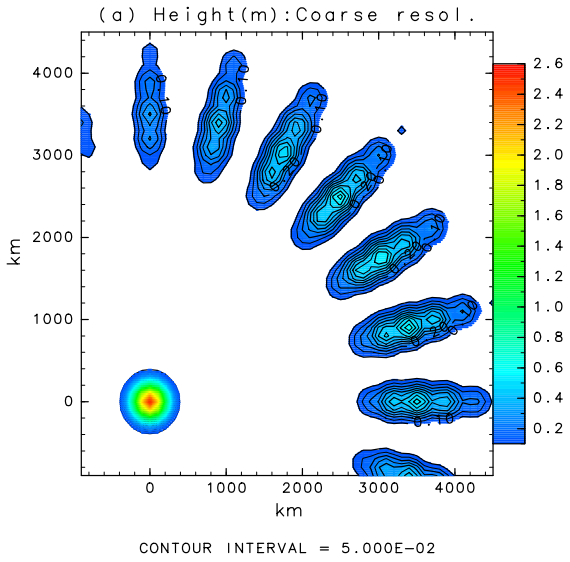
(a) Height(m):Coarse resol.
4000
3000
2000
1000
0
km
0
1000
2000
3000
4000
km
2.6
2.4
2.2
2.0
1.8
1.6
1.4
1.2
1.0
0.8
0.6
0.4
0.2
CONTOUR INTERVAL = 5.000E-02

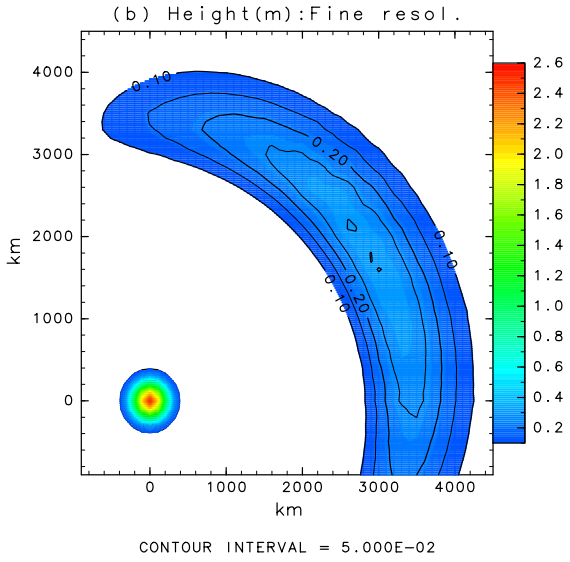
(b) Height(m):Fine resol.
4000
3000
2000
1000
0
km
0.10
0.20
0
1000
2000
3000
4000
km
2.6
2.4
2.2
2.0
1.8
1.6
1.4
1.2
1.0
0.8
0.6
0.4
0.2
CONTOUR INTERVAL = 5.000E-02

Figure 1

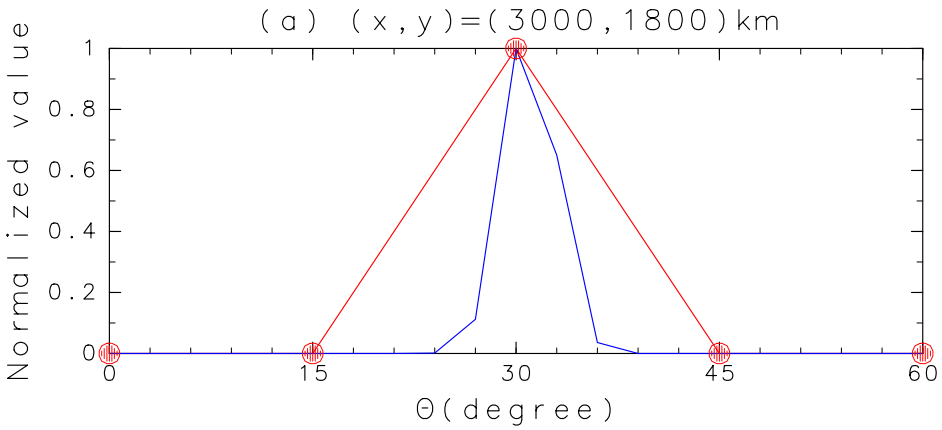
(a) (x,y)=(3000,1800)km
Normalized value
1
0.8
0.6
0.4
0.2
0
0
15
30
45
60
Θ(degree)

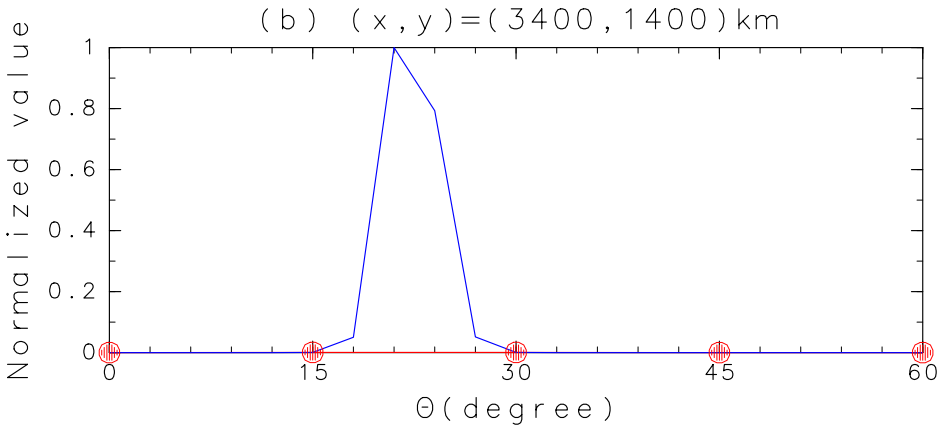
(b) (x,y)=(3400,1400)km
Normalized value
1
0.8
0.6
0.4
0.2
0
0
15
30
45
60
Θ(degree)

Figure 2

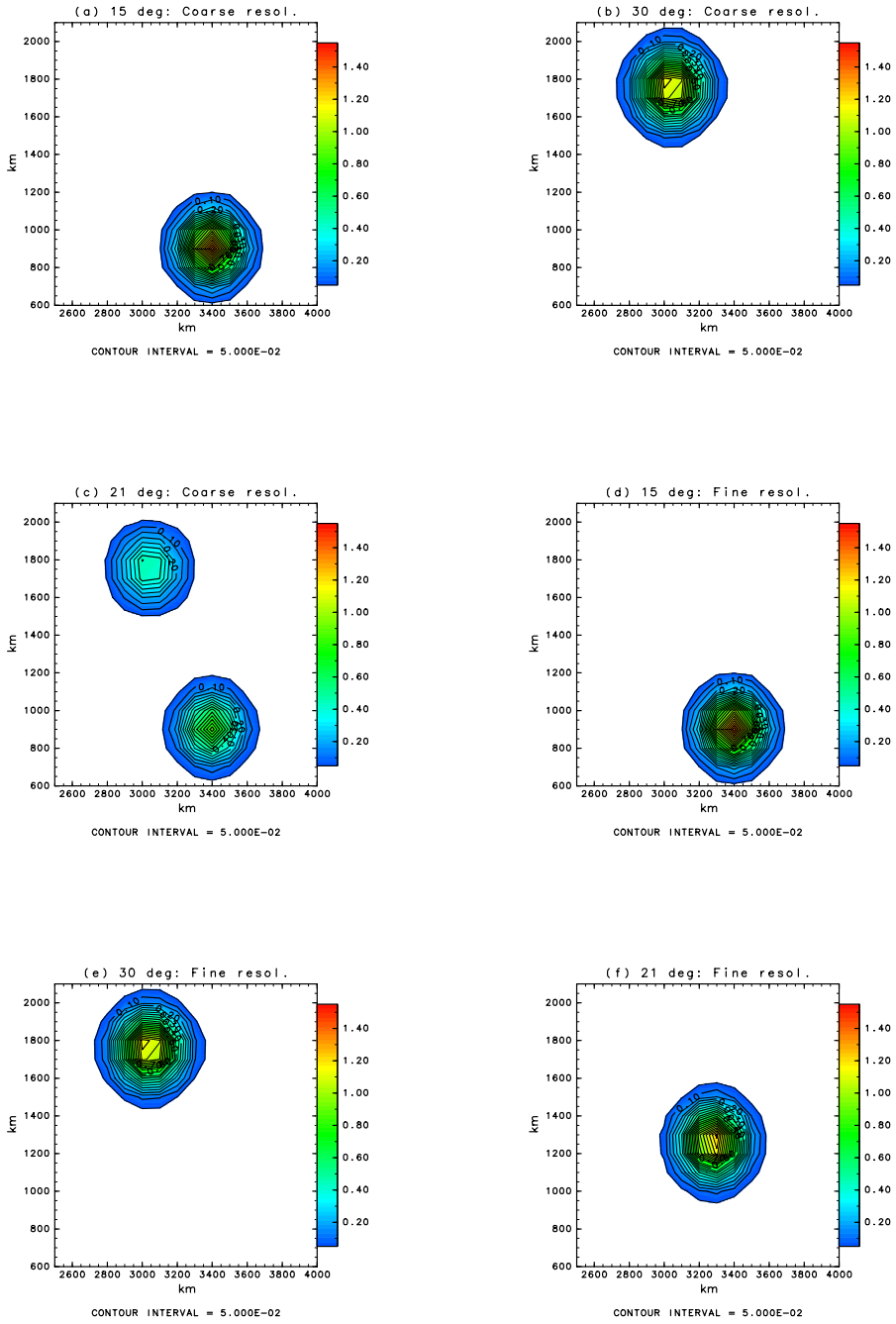
(a) 15 deg: Coarse resol.
(b) 30 deg: Coarse resol.
(c) 21 deg: Coarse resol.
(d) 15 deg: Fine resol.
(e) 30 deg: Fine resol.
(f) 21 deg: Fine resol.
km
2600 2800 3000 3200 3400 3600 3800 4000
600 800 1000 1200 1400 1600 1800 2000
0.20 0.40 0.60 0.80 1.00 1.20 1.40
CONTOUR INTERVAL = 5.000E-02

Figure 3

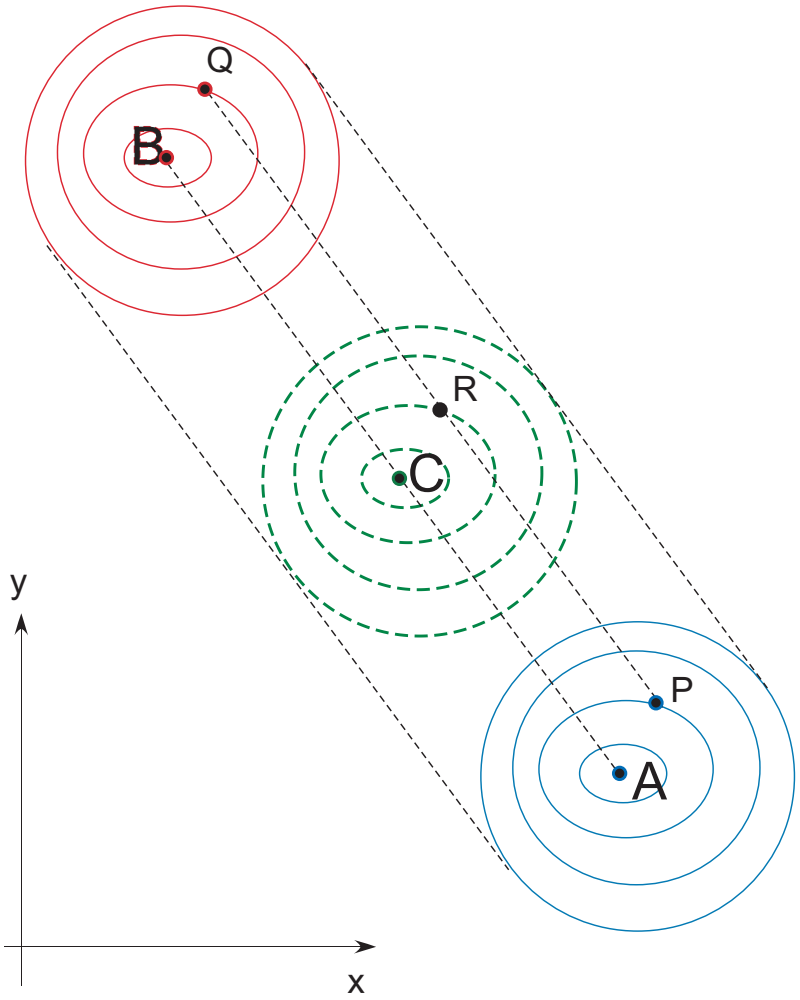

Figure 4

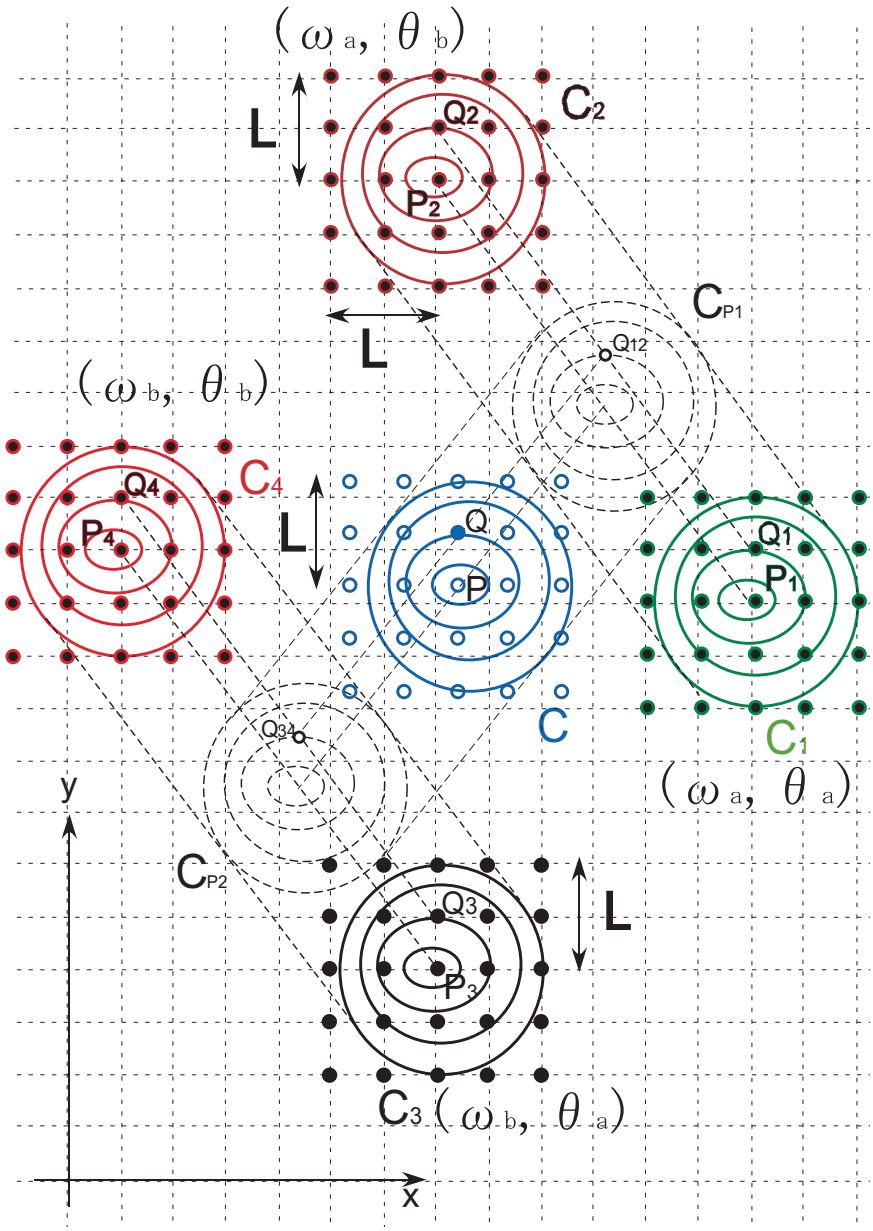
(ω a, θ b)
L
Q2
C2
P2
L
CP1
Q12
(ω b, θ b)
Q4
C4
P4
L
Q
P
C
Q1
P1
C1
Q34
(ω a, θ a)
y
CP2
Q3
L
P3
C3 (ω b, θ a)
x

Figure 5

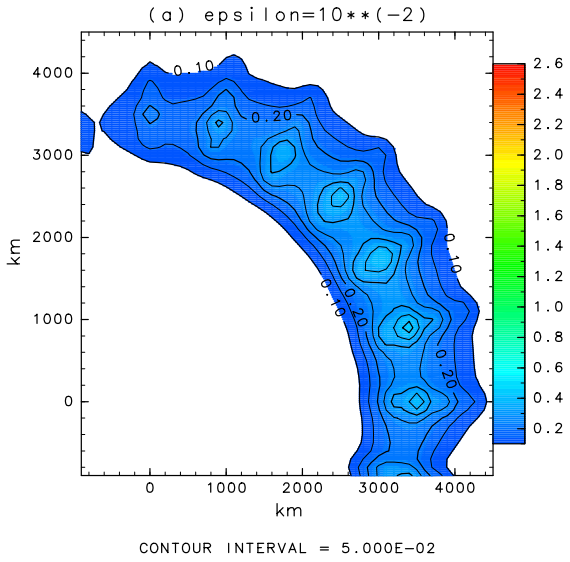
(a) epsilon=10**(-2)
4000
3000
2000
1000
0
km
0.10
0.20
0.10
0.20
0.20
0
1000
2000
3000
4000
km
2.6
2.4
2.2
2.0
1.8
1.6
1.4
1.2
1.0
0.8
0.6
0.4
0.2
CONTOUR INTERVAL = 5.000E-02

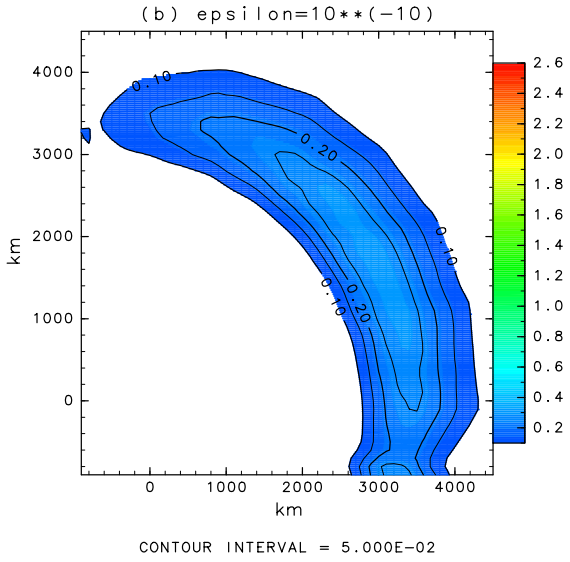
(b) epsilon=10**(-10)
4000
3000
2000
1000
0
km
0.10
0.20
0.10
0.20
0
1000
2000
3000
4000
km
2.6
2.4
2.2
2.0
1.8
1.6
1.4
1.2
1.0
0.8
0.6
0.4
0.2
CONTOUR INTERVAL = 5.000E-02

Figure 6

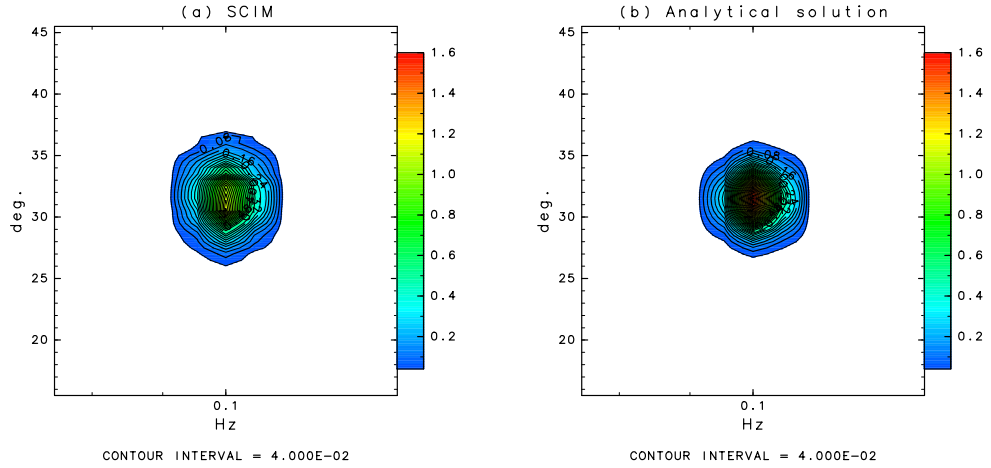
(a) SCIM
(b) Analytical solution
deg.
Hz
CONTOUR INTERVAL = 4.000E-02

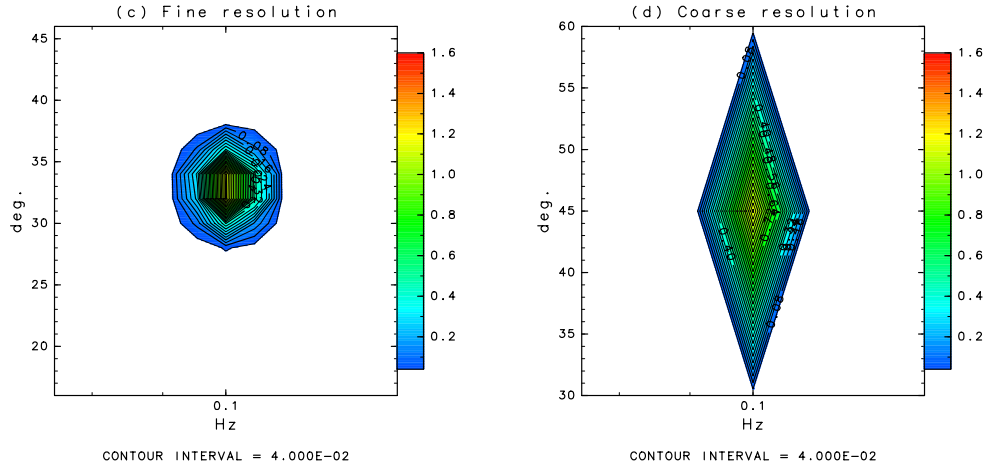
(c) Fine resolution
(d) Coarse resolution
deg.
Hz
CONTOUR INTERVAL = 4.000E-02

Figure 7

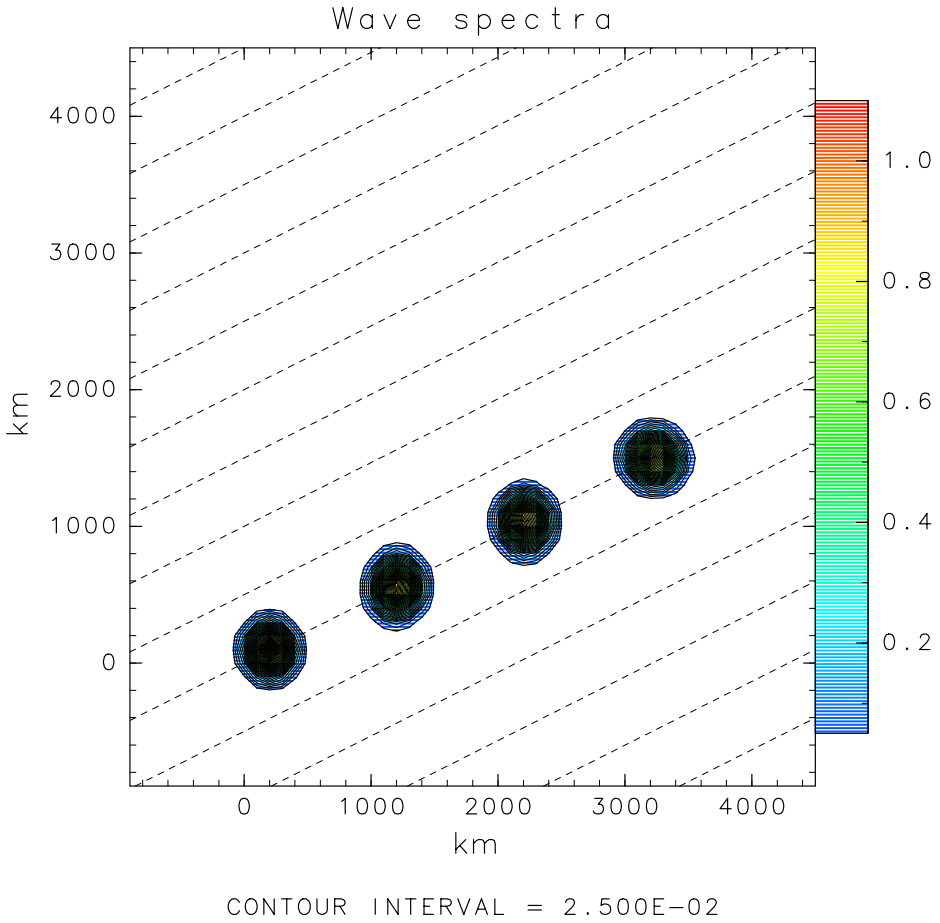
Wave spectra
4000
3000
2000
1000
0
km
0
1000
2000
3000
4000
km
1.0
0.8
0.6
0.4
0.2
CONTOUR INTERVAL = 2.500E-02

Figure 8

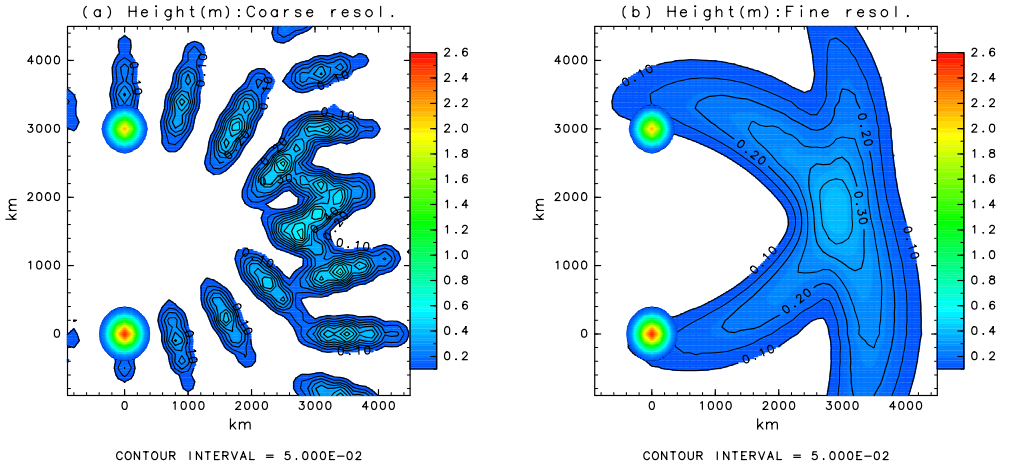
(a) Height(m):Coarse resol.
(b) Height(m):Fine resol.
km
CONTOUR INTERVAL = 5.000E-02

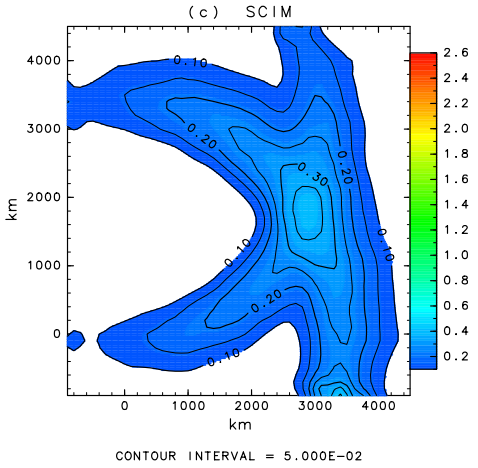
(c) SCIM
km
CONTOUR INTERVAL = 5.000E-02

Figure 9

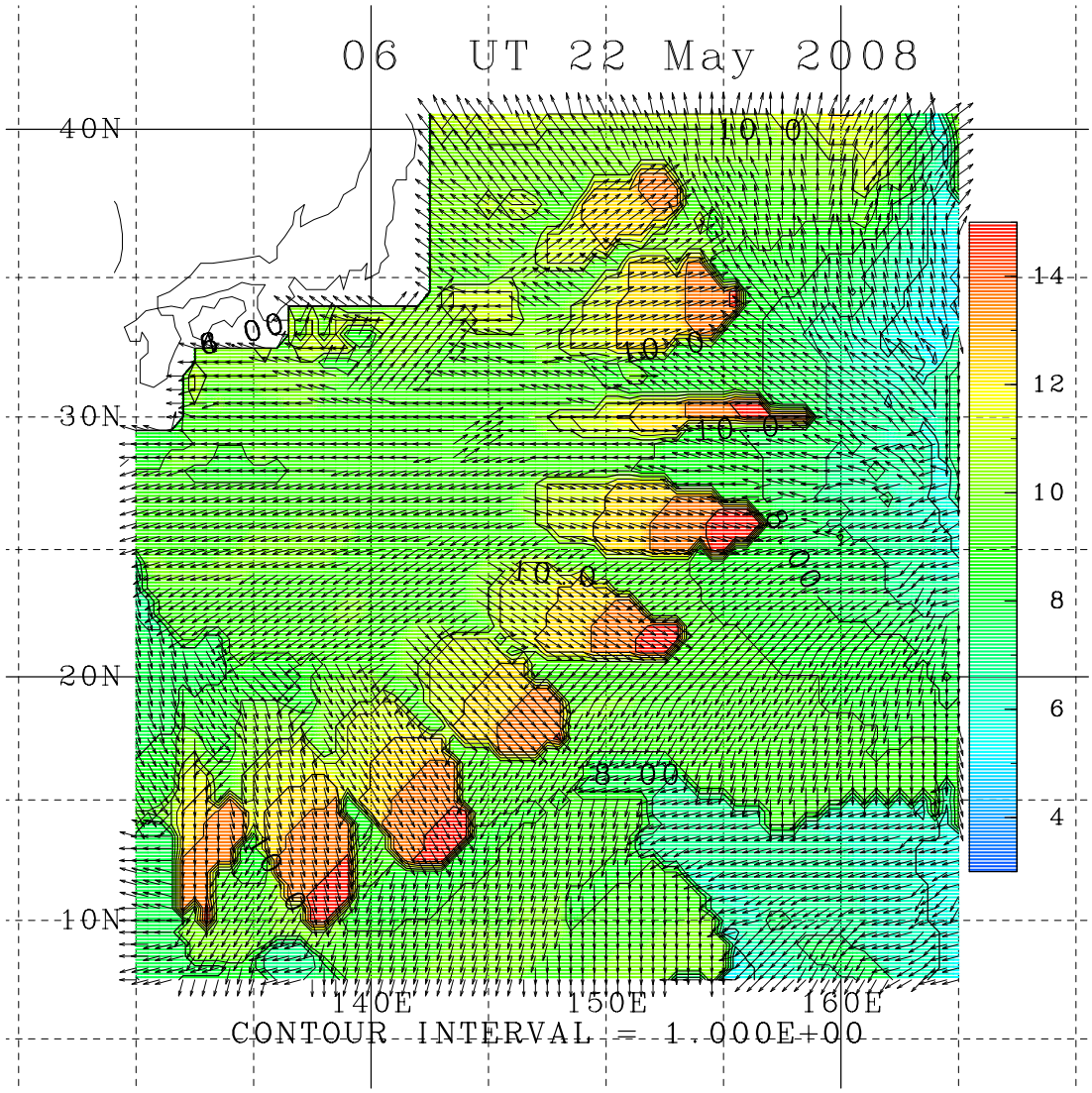
06 UT 22 May 2008
40N
30N
20N
10N
140E
150E
160E
14
12
10
8
6
4
CONTOUR INTERVAL = 1.000E+00

Figure 10

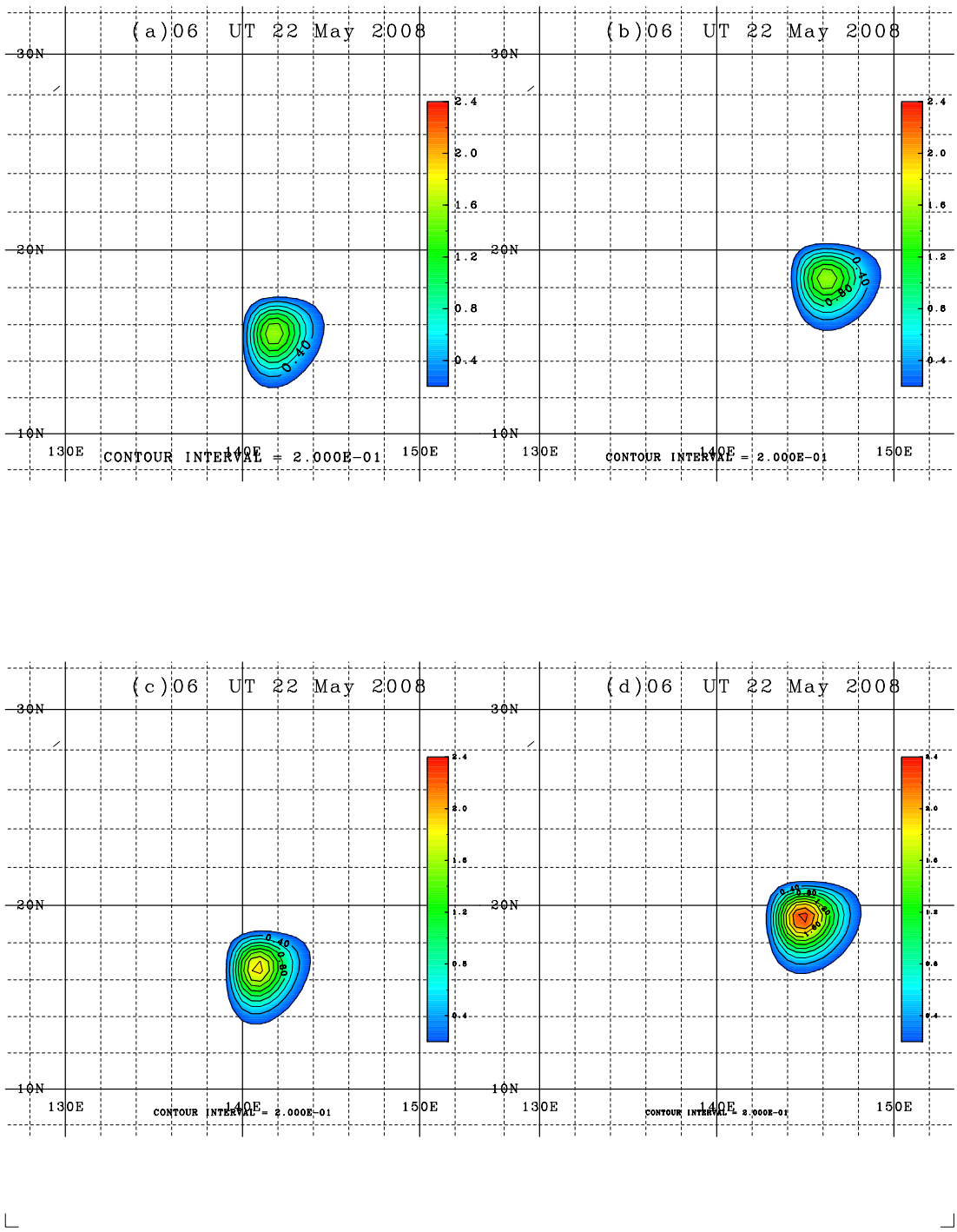
(a)06 UT 22 May 2008
(b)06 UT 22 May 2008
(c)06 UT 22 May 2008
(d)06 UT 22 May 2008
30N
20N
10N
130E
140E
150E
CONTOUR INTERVAL = 2.000E-01
2.4
2.0
1.6
1.2
0.8
0.4

Figure 11

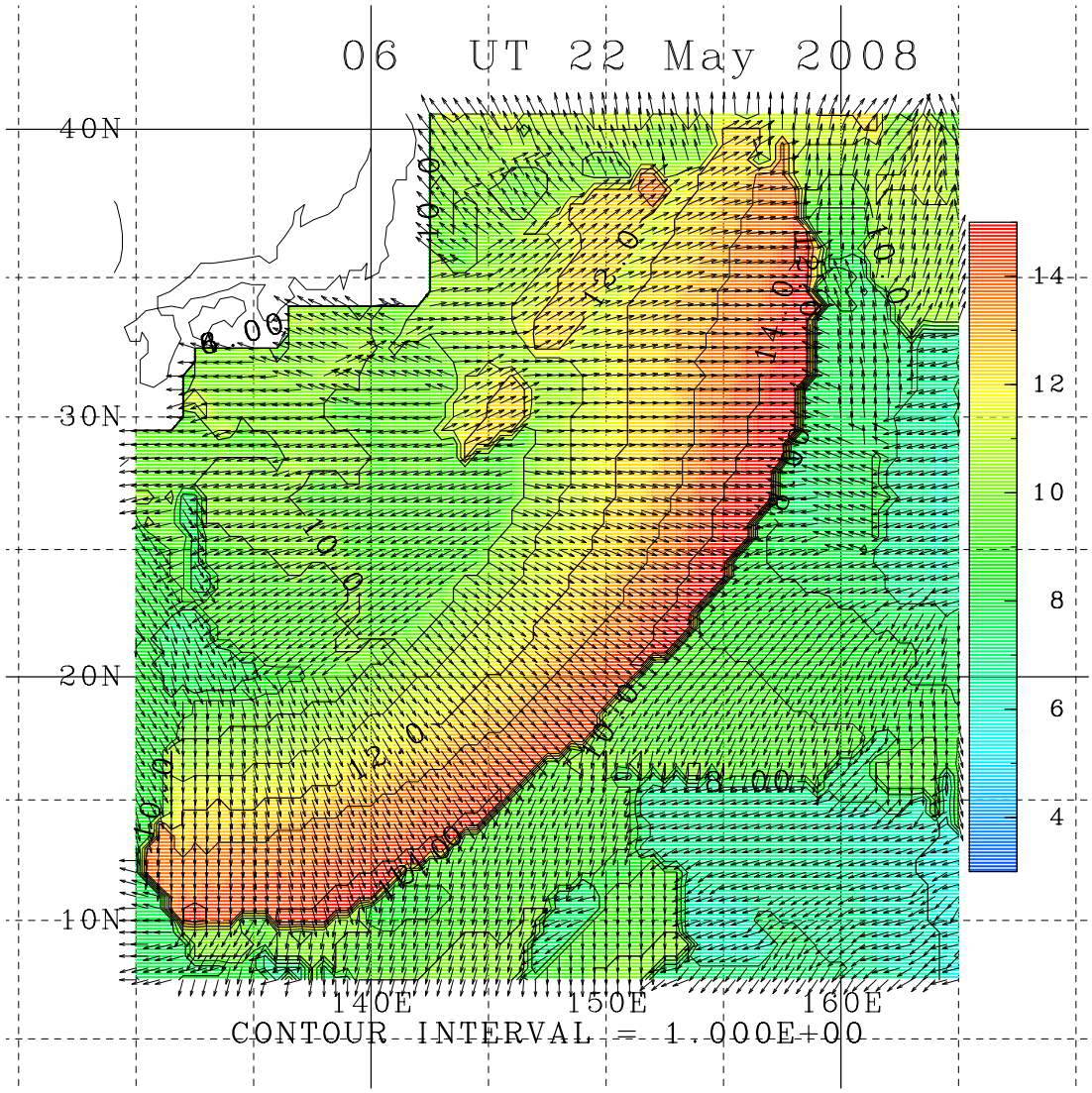
06 UT 22 May 2008
40N
30N
20N
10N
140E
150E
160E
14
12
10
8
6
4
CONTOUR INTERVAL = 1.000E+00

Figure 12

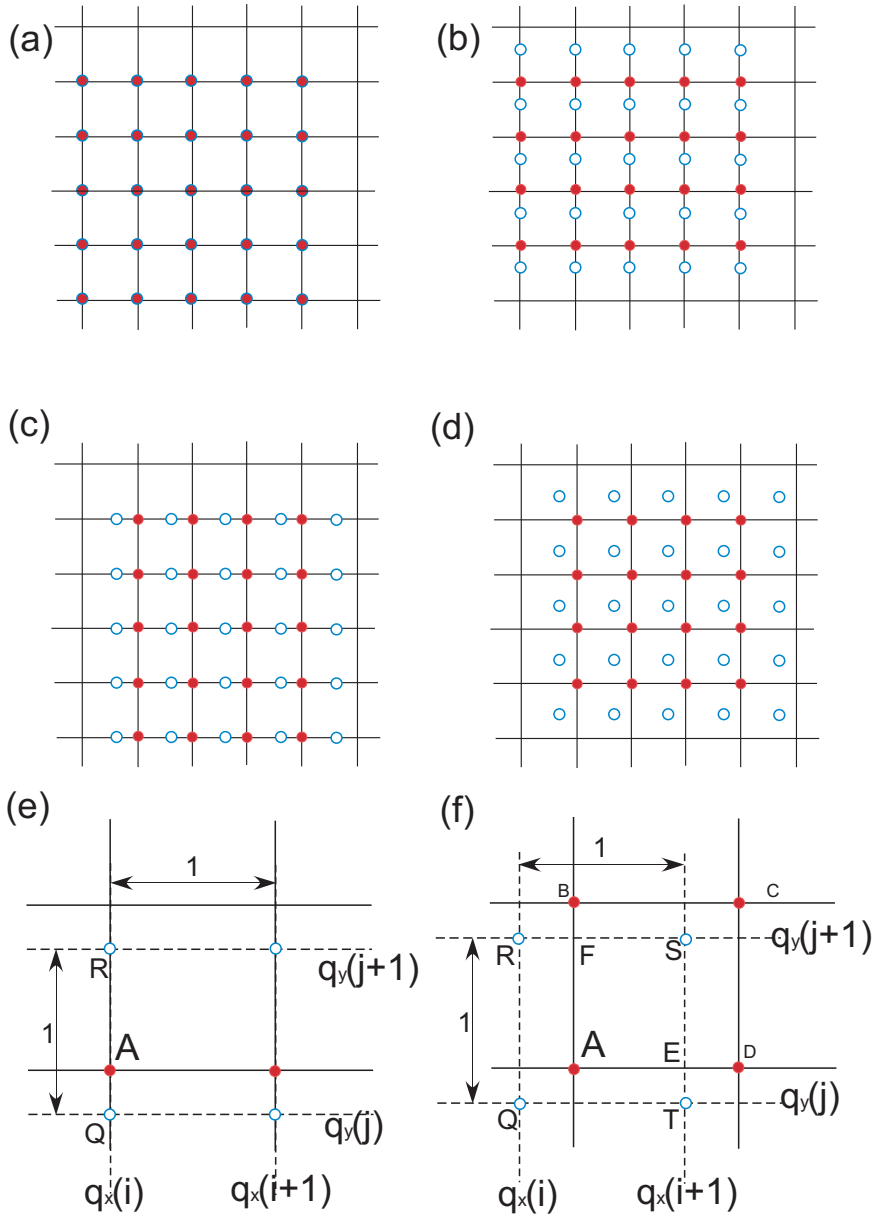
(a)
(b)
(c)
(d)
(e)
1
R
$q_y(j+1)$
1
A
Q
$q_y(j)$
$q_x(i)$
$q_x(i+1)$
(f)
1
B
C
R
F
S
$q_y(j+1)$
1
A
E
D
Q
T
$q_y(j)$
$q_x(i)$
$q_x(i+1)$

Figure 13